

# Metal insulator semiconductor solar cell devices based on a $\text{Cu}_2\text{O}$ substrate utilizing h-BN as an insulating and passivating layer

Onur Ergen,<sup>1,2,3</sup> Ashley Gibb,<sup>1,2,3</sup> Oscar Vazquez-Mena,<sup>1,2,3</sup> William Raymond Regan,<sup>1,2</sup> and Alex Zettl<sup>1,2,3,a)</sup>

<sup>1</sup>Department of Physics, University of California at Berkeley, Berkeley, California 94720, USA

<sup>2</sup>Materials Sciences Division, Lawrence Berkeley National Laboratory, Berkeley, California 94720, USA

<sup>3</sup>Kavli Energy Nanosciences Institute at the University of California, Berkeley, and the Lawrence Berkeley National Laboratory, Berkeley, California 94720, USA

(Received 19 December 2014; accepted 23 February 2015; published online 11 March 2015)

We demonstrate cuprous oxide ( $\text{Cu}_2\text{O}$ ) based metal insulator semiconductor Schottky (MIS-Schottky) solar cells with efficiency exceeding 3%. A unique direct growth technique is employed in the fabrication, and hexagonal boron nitride (h-BN) serves simultaneously as a passivation and insulation layer on the active  $\text{Cu}_2\text{O}$  layer. The devices are the most efficient of any  $\text{Cu}_2\text{O}$  based MIS-Schottky solar cells reported to date. © 2015 AIP Publishing LLC. [<http://dx.doi.org/10.1063/1.4914181>]

Cuprous oxide ( $\text{Cu}_2\text{O}$ ) has been investigated off and on as a possible non-toxic, low-cost, earth-abundant photovoltaic material for several decades.<sup>1–6</sup> Unfortunately,  $\text{Cu}_2\text{O}$  is exceedingly difficult to chemically dope, limiting its application for conventional p-n junctions.<sup>4–6</sup> In 1979, Olsen *et al.*<sup>1</sup> suggested that a high efficiency  $\text{Cu}_2\text{O}$  solar cell might be possible using either a metal insulator semiconductor Schottky (MIS-Schottky) configuration, or a heterojunction; both offered a highly attractive theoretical conversion efficiency of  $\sim 20\%$ .<sup>1–5</sup> The highest conversion efficiency for a  $\text{Cu}_2\text{O}$ -based system is 5.38%, reported for a heterojunction solar cell using undoped gallium oxide ( $\text{Ga}_2\text{O}_3$ ) as a buffer middle layer for Al-doped  $\text{ZnO}/\text{Cu}_2\text{O}$ .<sup>7,8</sup> However, in the 35 years since Olsen's prediction, no notable  $\text{Cu}_2\text{O}$ -based MIS-Schottky devices have been realized, presumably due to difficulties with highly sensitive surface states of  $\text{Cu}_2\text{O}$ .<sup>1–3,5–9</sup> There have been many reports of metal/ $\text{Cu}_2\text{O}$  Schottky junction solar cells, but even these cells struggle to achieve efficiencies over 2% due to dangling bonds on the surface and uncontrolled reduction of the  $\text{Cu}_2\text{O}$  on the surface to an undesirable copper-rich phase.<sup>1–3,7–15</sup>

We here demonstrate a unique direct growth technique utilizing copper and hexagonal boron nitride (h-BN) to create a stable MIS-Schottky solar cell structure. The h-BN layer serves simultaneously as a passivation and insulation layer on the active  $\text{Cu}_2\text{O}$  film; formation of an undesirable copper-rich interface layer is thus prevented. The resulting MIS-Schottky solar cell devices display high short circuit current density ( $J_{sc}$ ) and open circuit voltage ( $V_{oc}$ ) with a conversion efficiency as high as  $\sim 3.44\%$ . This is the highest efficiency yet reported for a  $\text{Cu}_2\text{O}$ -based MIS-Schottky solar cell device and a direct experimental demonstration of two-dimensional layer materials in energy conversion devices.

Figure 1 illustrates two related fabrication processes that we have employed for our  $\text{Cu}_2\text{O}$  MIS-Schottky structures, which we label as type 1 and type 2. The devices are constructed using 0.025 mm thick copper foil with a  $\sim 15$  nm thick h-BN layer grown by chemical vapor deposition

(CVD), (Figs. 1(a) and 1(b)).<sup>16</sup> Because h-BN grows on both sides of the copper foil, a light polishing is applied to the bottom layer to allow oxidation to proceed through the bottom surface (Fig. 1(c)).  $\text{Cu}_2\text{O}$  growth is performed with a standard two-step oxidation process to achieve larger grain size (Fig. 1(d)).<sup>17–22</sup> Next, an annealing step is performed at 850 °C for 2 h in 1 Torr  $\text{O}_2$  partial pressure in order to lower the defect density to improve mobility. High temperatures are necessary in order to convert copper to cuprous oxide, in the correct phase.<sup>5,10,17–20</sup> However, oxidation of thin copper foil at high temperatures is a challenging process due to its thermal expansion and crystallization behavior. Fortunately,

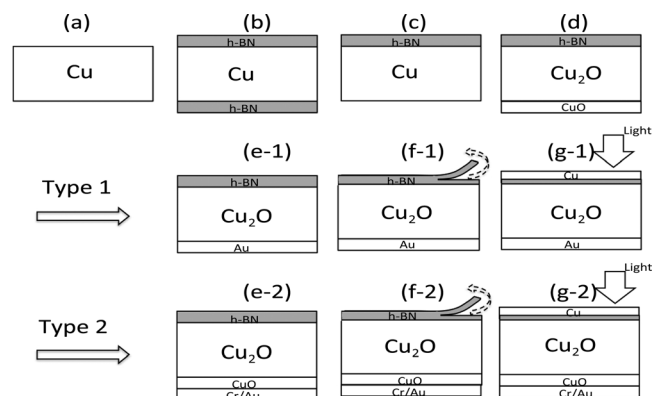


FIG. 1. Cross-sectional schematic diagram of  $\text{Cu}_2\text{O}$  based MIS cells, type 1 and type 2. A 15 nm thick h-BN layer deposited on 0.025 mm thick copper foil via CVD followed by applying a light polish to the bottom layer to remove h-BN from the back surface ((a)–(c)). The Cu foil is oxidized using a standard two-step oxidation process to form a  $\text{Cu}_2\text{O}$  layer (d). In this oxidation step, different carrier gases ( $\text{Ar}/\text{O}_2$ ,  $\text{N}_2$ , and  $\text{H}_2$ ) are introduced during cooling.  $\text{CuO}$  formation is only occurring at the bottom surface of the  $\text{Cu}_2\text{O}$ , not at the h-BN/ $\text{Cu}_2\text{O}$  interface. For type 1 devices, this  $\text{CuO}$  layer is removed by lightly polishing and 10 nm Au is deposited as a back contact (e-2). In step (f), the h-BN is exfoliated. As a final step, a 5 nm thick transparent Cu layer is deposited as a top contact. The process of a type 2 structure is identical to type 1, except step (e). In this step for the type 2 device,  $\text{CuO}$  is not polished and Cr/Au is deposited as a back contact (5 nm/10 nm), followed by annealing at 200 °C in an Ar environment. We achieve up to 2.3% and 3.44% efficiencies for type 1 and type 2 devices, respectively. In step (g), illumination direction is shown by the arrows.

<sup>a)</sup>Electronic mail: azettl@berkeley.edu

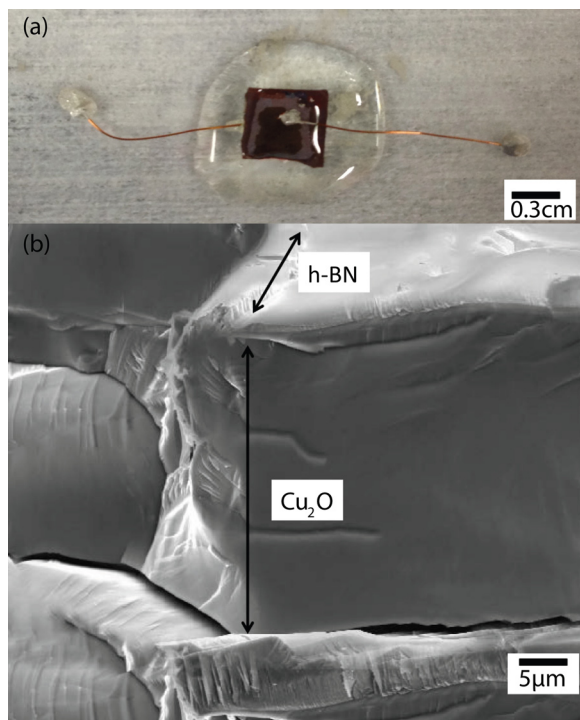


FIG. 2. (a) Optical photograph of complete device structure of MIS-Schottky solar cell. (b) Cross sectional SEM image of h-BN on  $\text{Cu}_2\text{O}$ . There is no  $\text{CuO}$  formation on the h-BN/ $\text{Cu}_2\text{O}$  interface. The boron nitride layer remains intact after  $\text{Cu}_2\text{O}$  growth. (See supplementary material for performed Raman spectroscopy.)<sup>31</sup>

the relatively thick hexagonal boron nitride layer provides additional mechanical strength to the foil during growth and allows for easy handling of the material after growth. During step (d), following the growth and annealing steps, the substrates are slowly cooled in one of three different gaseous environments: argon/oxygen ( $\text{Ar}/\text{O}_2$ ), nitrogen ( $\text{N}_2$ ), or hydrogen ( $\text{H}_2$ ). By introducing different gas environments, we induce distinct passivation layers on the top surface of the  $\text{Cu}_2\text{O}$ . This passivation process is enabled by the h-BN layer. The h-BN layer also obviates the traditional wet etching process for a possible cupric oxide ( $\text{CuO}$ ) layer on the top surface of  $\text{Cu}_2\text{O}$ .<sup>20,21</sup> Since in our process a cupric oxide ( $\text{CuO}$ ) layer is formed only on the bottom surface of the oxidized foil, the top surface being protected by the existing h-BN layer (Fig. 2(b)).

To produce a type 1 device, the bottom surface of the foil following conversion is lightly polished to remove the  $\text{CuO}$  layer followed by  $\sim 10$  nm thick Au film deposition as a back contact (Fig. 1(e-1)). To produce an MIS cell, the h-BN layer is thinned by exfoliation, using the standard scotch tape and polydimethylsiloxane (PDMS) stamp techniques, decreasing the h-BN thickness in a range of  $\sim 1$  nm– $\sim 6$  nm (Fig. 1(f-1)). This exfoliation process is crucial for forming a proper MIS device structure utilizing h-BN as an insulator layer. As a final step, a  $\sim 5$  nm thick transparent copper layer is evaporated on the top surface of the exfoliated h-BN layer as a top contact. The composition of a type 2 structure is identical to type 1, except for step (e). In this step, for type 2,  $\text{CuO}$  is not polished off and Cr and Au are deposited, 5 nm and 10 nm thick, respectively, as a back contact, followed by an annealing process at  $200^\circ\text{C}$  in an Ar environment (Fig.

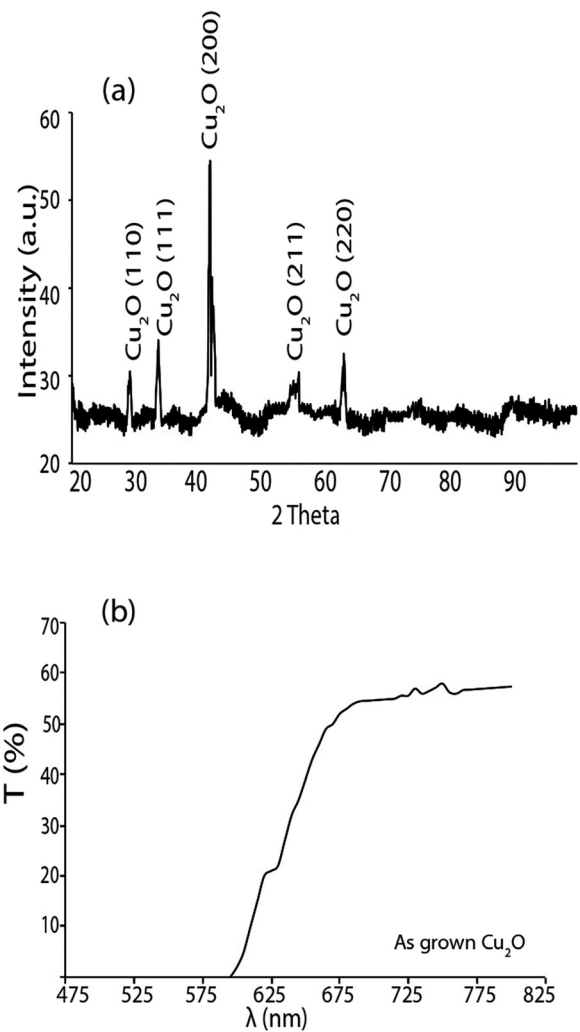


FIG. 3. (a) X ray pattern of as grown  $\text{Cu}_2\text{O}$ . The sharp diffraction peaks indicate high quality  $\text{Cu}_2\text{O}$ . (b) Short-scan of optical transmittance spectra, at room temperature, indicates energy band gap equal to  $\sim 2.08$  eV using absorption fitting method. Both figures show high quality  $\text{Cu}_2\text{O}$  material formation.

1(e-2)). This annealing process helps Cr diffuse into the  $\text{CuO}$  layer to create a degenerately doped region.

Fig. 2(a) shows an optical image of the complete device, and Fig. 2(b) shows a cross-sectional SEM image of h-BN/ $\text{Cu}_2\text{O}$  at step (d) in Fig. 1. Fig. 2(b) confirms that there is no  $\text{CuO}$  formation on the h-BN/ $\text{Cu}_2\text{O}$  interface. The quality of cuprous oxide is characterized by X-ray diffraction (XRD) (Fig. 3(a)) and optical transmission spectroscopy (Fig. 3(b)). As seen in Fig. 3(a), the sharp diffraction peaks indicate high quality  $\text{Cu}_2\text{O}$ . The h-BN formation seems to prevent unwanted  $\text{CuO}$  formation on the top surface of  $\text{Cu}_2\text{O}$  layer, which correlates with Fig. 2(b). The optical transmittance spectra in Fig. 3(b) indicate a band-gap of  $\sim 2.08$  eV ( $\lambda = 595$  nm) using the standard absorption fitting method. This value is consistent with band gap values reported in literature of  $\text{Cu}_2\text{O}$  (2.0–2.1 eV).<sup>4,5,20</sup> The depth of oxidation is also easily controlled by varying the growth time. For instance, a buried  $\text{Cu}/\text{Cu}_2\text{O}$  layer is readily achieved using short growth times (Figure S1).<sup>31</sup>

In order to verify that the h-BN layer remains intact after  $\text{Cu}_2\text{O}$  growth, we employ Raman spectroscopy. The  $\text{Cu}_2\text{O}$  substrate is slowly etched using saturated nitric acid, and the

h-BN is transferred to a Si/SiO<sub>2</sub> substrate for analysis. As seen in Figure S2, the signature B-N vibrational E<sub>2g</sub> peak of h-BN is observed at 1366.7 cm<sup>-1</sup>.<sup>16,22,31</sup> The thickness of h-BN on devices is estimated via capacitance measurements. High-frequency (1MHz) capacitance-voltage (C-V) characteristics are measured at room temperature using HP4192 A LCR meter. Capacitance, which is inversely proportional to the thickness of the dielectric, is measured on exfoliated h-BN/Cu<sub>2</sub>O substrates by probing during electrical measurements. The exfoliation process makes the h-BN layer thin enough to allow the tunneling current transport process. We estimate the thinnest h-BN layer to be approximately 2 nm from electrical response analysis. The two other thicker layers were approximately 5 nm apart as demonstrated by decreasing the dielectric capacitance in the C-V curve; which is also consistent with atomic force microscopy (AFM) measurements (Figs. S6 and S8).<sup>31</sup>

Fig. 4(a) shows I-V curves of several different MIS solar cells under AM1.5G illumination. It is clear that the electronic properties of the solar cells are directly affected by the kind of cooling gas used during synthesis. Thin films of polycrystalline Cu<sub>2</sub>O are expected to have many dangling bonds, which act as an interface recombination center on the grain

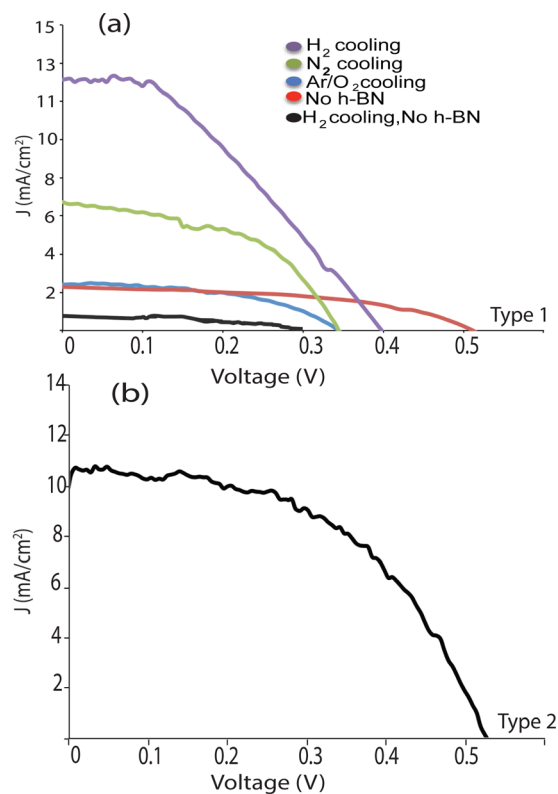


FIG. 4. (a) J-V curves of type 1 device structures show remarkable short circuit increases with respect to Cu/Cu<sub>2</sub>O devices utilizing different cooling gas environments, Ar/O<sub>2</sub>, N<sub>2</sub>, and H<sub>2</sub>, respectively, N<sub>2</sub> and H<sub>2</sub> cooling remarkably increase  $J_{sc}$ . The overall photovoltaic cell efficiency of the device cooled in hydrogen is approximately 2.3% with 12.1 mA/cm<sup>2</sup> current density over an area of 0.35 cm by 0.4 cm. This graph indicates that h-BN plays a very important role in improving device performance because the devices fabricated without h-BN layer are not favorable. (b) J-V curve of type 2 device structure indicates having CuO and Cr/Au combination at the back surface of Cu<sub>2</sub>O helps to increase  $V_{oc}$  and solar conversation efficiency. The efficiency of this device is 3.44% with  $V_{oc}$  0.52 V.

surface.<sup>12,13,23–25</sup> The improvement of the short circuit current density could be a clear signature of reducing interface states and increasing carrier collection efficiency, which is a sign of active passivation while trapping hydrogen and nitrogen between interfaces (Fig. 4(a)). The improvement of front and rear surface recombination is also shown in the external quantum efficiency measurement (Fig. S7).<sup>31</sup> Another important characteristic of the h-BN layer is that it prevents the formation of a copper-rich interface layer, which is linked to lowered efficiency in metal/Cu<sub>2</sub>O devices due to tuning of the work function and is correlated with low open circuit voltage ( $V_{oc}$ ).<sup>5,10,11,20</sup> We also suspect monolayer nitrogen doping under the h-BN layer, which controls Fermi level pinning at the interface (Fig. 4(a)).<sup>1–5,23–25</sup>

The overall photovoltaic cell efficiency of the type 1 device produced in hydrogen is approximately 2.3% with 12.1 mA/cm<sup>2</sup> current density over an area of 0.35 cm by 0.4 cm. The h-BN appears to play an essential role in improving device performance, as the devices fabricated without h-BN layer are consistently less responsive to cooling gases. Non-h-BN devices also display a marked decline in device performance, especially when hydrogen gas is introduced into the system due to Cu<sub>2</sub>O surface reduction. However, we have observed  $V_{oc}$  increase in the device with O<sub>2</sub> cooling due to increase in grain dimensions, as predicted in literature.<sup>18–20,23–26</sup>

For selected type 2 devices, we employ Cr/Au as a contact layer on the back surface of the Cu<sub>2</sub>O/CuO interface. Later, the device is annealed at 200 °C in an Ar environment to allow Cr diffusion into the cupric oxide, which results in an improvement in  $V_{oc}$ . Although more experiments are needed to clarify the contribution of various interfaces, it is likely that the diffusion of Cr into the Cu<sub>2</sub>O/CuO interface provides an additional band offset leading to an increase in  $V_{oc}$ . No improvement has been observed in type 1 devices with a Cr layer. Despite a small increase in resistivity and a decrease in the short circuit current ( $I_{sc}$ ), the overall efficiency of such a type 2 device is improved to 3.44%, in contrast to ~2% we observed previously for Cu<sub>2</sub>O based Schottky devices. No anti-reflection coating is necessary for this improvement (Fig. 4(b)). 3.44% is the highest efficiency reported for Cu<sub>2</sub>O based Schottky solar cells.

We have observed that for both type 1 and type 2 devices a non-uniform thickness of the h-BN layer influences the current tunneling ability of the device, and hence the noise response. Variable thickness h-BN results in the fill factor (FF) directly depending on the rate of bias sweeping. We note that fast voltage sweep rates (1 ms) reflect very different FF than slower (~1 s) voltage sweep rates and increased FF affects the apparent efficiency of the device (Figure S4).<sup>27,31</sup>

In summary, we have demonstrated a versatile route toward the controllable synthesis of a cuprous oxide solar cell, with an efficiency of 3.44%, using a surface sensitive thin film of h-BN and a back CuO layer to increase the band offset. The ability to control passivation of the non-radiative recombination centers and donor-like defects are suggested, in addition to inhibiting reduction of the Cu<sub>2</sub>O surface, which is another contributor in blocking out the majority carrier flow to reduce the reverse saturation current.<sup>1–3,28–30</sup> This technique has advantageous features including easy

fabrication, the ability to use thinner Cu foil, and prevention of an unwanted CuO layer. It is also highly generic and has great potential to construct an exquisite passivation on the sensitive surfaces in combination with hydrogen and nitrogen treatment. We also note that in the current work we evaporated top contacts of sufficient thicknesses to avoid pinhole shorts. In our future work, we hope to optimize the contacts and achieve even higher efficiencies. In the future, this technique might be used to design high efficiency, low cost, and stable solar cell structures.

*Methods:* CVD h-BN was grown on 0.025 mm thick copper foil (99.999% Puratronic, Alfa Aesar), which was then cut into 0.2 cm by 0.3 cm pieces. The back surface of the sample was mechanically polished to increase the bottom to top oxidation rate. The two step thermal oxidation process was carried out for 30 min at 950 °C with O<sub>2</sub> partial pressure of 2.7 Torr followed by 2 h at 850 °C with O<sub>2</sub> partial pressure of 1 Torr. After the Cu<sub>2</sub>O growth, the chamber and all gas lines were purged with 200 sccm of argon to remove all the O<sub>2</sub> from the system. Next, only one of the three transport gases Ar/O<sub>2</sub>, N<sub>2</sub>, and H<sub>2</sub> was introduced in the chamber during the cooling process under a partial pressure of 1 Torr. After cooling, the back surface of the substrate was slightly polished, for type I only, followed by deposition of a 10 nm Au film and bonding of a thin copper wire. Then, the sample was carefully attached to a glass slide using an epoxy glue. The sample was exfoliated using a combination of scotch tape and PDMS stamp techniques. Finally, the substrate was loaded into a thermal evaporator for the deposition of a ~5 nm Cu layer as a top contact electrode.

This research was supported in part by the Office of Energy Research, Materials Sciences and Engineering Division of the U.S. Department of Energy under Contract No. DE-AC02-05CH11231, which provided for the design of the experiment and Raman spectroscopy characterization; the National Science Foundation within the Center of Integrated Nanomechanical Systems, under Grant No. EEC-0832819, which provided for photovoltaic response characterization; and by the Office of Naval Research (MURI) under Grant No. N00014-09-1066, which provided for graphene growth and device assembly. O.E. acknowledges the support of SoloPower Systems, Inc.,

through X-ray characterization and the support of Professor Paul Alivisatos's group through quantum efficiency measurements.

- <sup>1</sup>L. Olsen, R. Bohara, and M. Urie, *Appl. Phys. Lett.* **34**, 47–49 (1979).
- <sup>2</sup>L. Olsen, F. Addis, and W. Miller, *Sol. Cells* **7**, 247–279 (1982).
- <sup>3</sup>E. Y. Wang, D. Trivich, R. J. Komp, I-F. Huang, and D. J. Brinker, in *14th Photovoltaic Specialists Conference* (1980), Vol. 1, pp. 458–461.
- <sup>4</sup>A. Rakhshani, *Solid-State Electron.* **29**, 7–17 (1986).
- <sup>5</sup>A. Mittiga, E. Salza, F. Sarto, M. Tucci, and R. Vasanthi, *Appl. Phys. Lett.* **88**, 163502 (2006).
- <sup>6</sup>Y. Tsur and I. Riess, *Phys. Rev. B* **60**(11), 8138 (1999).
- <sup>7</sup>T. Minami, Y. Nishi, and T. Miyata, *Appl. Phys. Express* **6**(4), 044101 (2013).
- <sup>8</sup>Y. S. Lee, D. Chua, R. E. Brandt, S. C. Siah, J. V. Li, J. P. Mailoa, S. W. Lee, R. G. Gordon, and T. Buonassisi, *Adv. Mater.* **26**, 4704–4710 (2014).
- <sup>9</sup>K. Akimoto, S. Ishizuka, M. Yanagita, Y. Nawa, G. K. Paul, and T. Sakurai, *Sol. Energy* **80**(6), 715–722 (2006).
- <sup>10</sup>T. Minami, Y. Nishi, T. Miyata, and J. Nomoto, *Appl. Phys. Express* **4**, 062301 (2011).
- <sup>11</sup>C. Xiang, G. M. Kimball, R. L. Grimm, B. S. Brunschwig, H. A. Atwater, and N. S. Lewis, *Energy Environ. Sci.* **4**(4), 1311–1318 (2011).
- <sup>12</sup>R. Iwanowski and D. Trivich, *Sol. Cells* **13**, 253–264 (1985).
- <sup>13</sup>R. Iwanowski and D. Trivich, *Radiat. Eff.* **76**, 87–92 (1983).
- <sup>14</sup>R. N. Briskman, *Sol. Energy Mater. Sol. Cells* **27**, 361–368 (1992).
- <sup>15</sup>Y. Abdu and A. Musa, *Bayero J. Pure Appl. Sci.* **2**, 8–12 (2009).
- <sup>16</sup>A. L. Gibb, N. Alem, J. H. Chen, K. J. Erickson, J. Ciston, A. Gautam, M. Linck, and A. Zettl, *J. Am. Chem. Soc.* **135**(18), 6758–6761 (2013).
- <sup>17</sup>J. A. Assimos and D. Trivich, *J. Appl. Phys.* **44**(4), 1687–1693 (1973).
- <sup>18</sup>D. Trivich, E. Y. Wang, R. J. Komp, and A. S. Kakar, in *Proceedings of the 13th IEEE Photovoltaic Specialists Conference*, Washington, DC (1978).
- <sup>19</sup>D. Trivich, E. Y. Wang, and R. J. Komp, Final Report, 1 October 1975 to 31 March 1978, Wayne State University, Detroit, MI, 1978.
- <sup>20</sup>F. Biccari, Ph.D. thesis, Sapienza – University of Rome, 2009.
- <sup>21</sup>M. Clavaguera-Mora, J. Tournon, J. Rodriguez-Viejo, and N. Clavaguera, *J. Alloys Compd.* **377**, 8–16 (2004).
- <sup>22</sup>I. Babich, *Theor. Exp. Chem.* **8**, 594–595 (1974).
- <sup>23</sup>S. Ishizuka, S. Kato, Y. Okamoto, T. Sakurai, K. Akimoto, N. Fujiwara, and H. Kobayashi, *Appl. Surf. Sci.* **216**(1), 94–97 (2003).
- <sup>24</sup>Y. Okamoto, S. Ishizuka, S. Kato, T. Sakurai, N. Fujiwara, H. Kobayashi, and K. Akimoto, *Appl. Phys. Lett.* **82**(7), 1060–1062 (2003).
- <sup>25</sup>S. Poulston, P. Parlett, P. Stone, and M. Bowker, *Surf. Interface Anal.* **24**, 811–820 (1996).
- <sup>26</sup>J. Y. Kim, J. A. Rodriguez, J. C. Hanson, A. I. Frenkel, and P. L. Lee, *J. Am. Chem. Soc.* **125**, 10684–10692 (2003).
- <sup>27</sup>D. Willett and S. Kuriyagawa, in *Conference Record of the Twenty Third IEEE Photovoltaic Specialists Conference* (IEEE, 1993), pp. 495–500.
- <sup>28</sup>L. C. Olsen, *Solid-State Electron.* **20**, 741–751 (1977).
- <sup>29</sup>M. A. Green and R. Godfrey, *Appl. Phys. Lett.* **29**, 610–612 (1976).
- <sup>30</sup>H. Card and E. Yang, *Appl. Phys. Lett.* **29**, 51–53 (1976).
- <sup>31</sup>See supplementary material at <http://dx.doi.org/10.1063/1.4914181> for details of material characterization, photovoltaic measurement, and electrical characterization.